THE NASA GSFC MEMS COLLOIDAL THRUSTER

Eric H. Cardiff*, Brian G. Jamieson†, Peter C. Norgaard‡, and Ariane B. Chepko§
NASA Goddard Space Flight Center
Greenbelt, MD 20771

A number of upcoming missions require different thrust levels on the same spacecraft. A highly scaleable and efficient propulsion system would allow substantial mass savings. One type of thruster that can throttle from high to low thrust while maintaining a high specific impulse is a Micro-Electro-Mechanical System (MEMS) colloidal thruster. The NASA GSFC MEMS colloidal thruster has solved the problem of electrical breakdown to permit the integration of the electrode on top of the emitter by a novel MEMS fabrication technique. Devices have been successfully fabricated and the insulation properties have been tested to show they can support the required electric field. A computational finite element model was created and used to verify the voltage required to successfully operate the thruster. An experimental setup has been prepared to test the devices with both optical and Time-Of-Flight diagnostics.

Introduction

A number of potential NASA missions require very precise attitude control with thrusts as low as 0.1 μN. Many of these upcoming missions use interferometers as part of the instrumentation, and the science results are therefore sensitive to the position of the spacecraft with respect to one another. Some of these potential missions are the Laser Interferometer Space Antenna (LISA), Micro-Arc second X-ray Interferometer Mission (MAXIM), Space Interferometer Mission (SIM), and Terrestrial Planet Finder (TPF)[1,2,3,4]. "Drag-free" missions also require propulsion systems to eliminate noise from gravitational disturbances. An example of this type mission is the Gravity Probe B mission[5]. A MEMS colloidal thruster is one type of thruster that could produce the precise thrust required for these types of missions.

Maneuvers for these missions can be roughly grouped in two broad categories. The first group is large attitude adjustments and/or drag compensation that requires thrust between 1-100 mN. The second category is disturbance reduction maneuvers and/or precise positioning maneuvers that require thrusts between 1 and 100 μN. A thrust range of 1 μN to 100 mN from one thruster could allow the propulsion system mass to be decreased by several factors.

Developing the thruster as a Micro- Electro-Mechanical Systems (MEMS) device on a silicon wafer allows large numbers of arrays to be manufactured cheaply and rapidly, and will allow greater emitter density to be used, thereby extending the thrust range to cover the range from 1 μN to 100 mN. In addition, the colloidal thruster is particularly well suited to micro-fabrication, as the associated smaller dimensions reduce the voltages required for operation.

The primary challenge in designing a MEMS electric thruster is the development of insulation between the accelerating electrodes and the emitter[6]. Attempts by other researchers to develop this type of thruster failed because of problems with electrical breakdown of the insulation[7,8].

Colloidal Thruster Theory

The colloidal thruster is an electrostatic propulsion technology. Thrust is produced by the electrostatic acceleration of small charged liquid droplets. The emitter has traditionally been a

* Propulsion Engineer, Senior Member
† Electronics Engineer, Member
‡ Student Intern, U. of Washington, Student Member
§ Co-op student , Purdue Univ., Student Member

small hypodermic needle that is biased to a potential of several kilovolts. An electrode with an opposite electric potential is placed above this emitter needle. A conductive ionic solution present in the needle is pulled towards the electrode in a characteristic cone shape. This cone shape was first observed in 1914 by Zeleny[9]. Extensive work was done on colloid thrusters through the 1960's, but these thrusters required voltage on the order of 10 kV[10].

The fluid cone shape was comprehensively described and characterized by G. I. Taylor in 1965[11], and is therefore commonly referred to as a "Taylor cone". The Taylor cone is formed by the interaction of the electrostatic field and the surface tension. At a critical diameter of the cone, it becomes unstable and breaks down into a stream of individual droplets. Charge concentration at the fluid surface gives these droplets a net charge. Thrust is produced as these droplets are accelerated away from the emitter by the electric field.

A schematic of the traditional setup of a needle colloidal thruster is shown in Figure 1. The Space Technology 7 mission uses this type of colloidal thruster as fabricated by Busek Co. Inc. The ST7 colloid thruster is composed of 8 thrusters arranged in 2 clusters, with 6 needles per thruster. Each thruster is capable of producing between 2 and 20 mN each, in increments of 0.1 mN, with thrust noise an order of magnitude less than the increment[13].

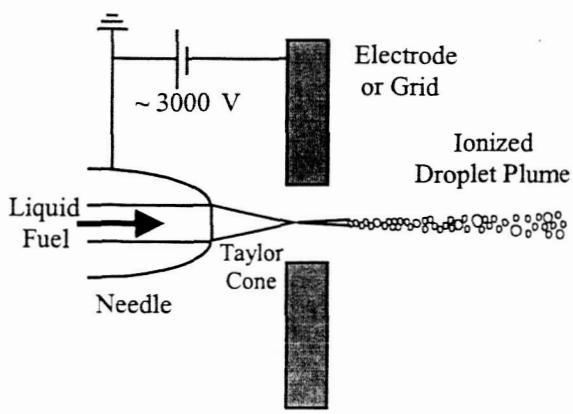

Figure 1. Traditional "needle" colloidal thruster.

Thruster Fabrication

A process was developed to manufacture the MEMS thrusters and several prototypes have been fabricated. An example of the prototype device showing a number of emitters with the surrounding silicon dioxide lattice structure is shown in Figure 2. The insulation was patterned around the emitter hole to allow the electrode to contact the body of the thruster without causing electrical breakdown. Several different insulation patterns were tested to compare the structural durability and the electrical breakdown characteristics.

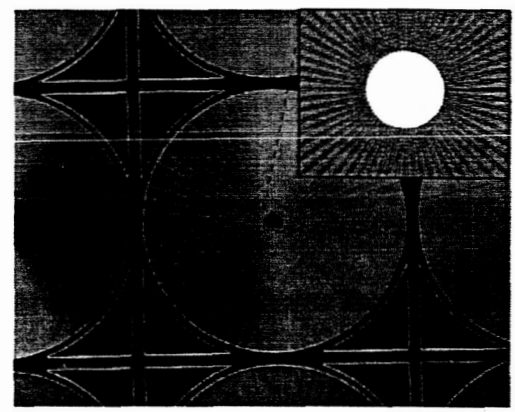

Figure 2: Image of the colloidal thruster emitter with a close-up of the insulation.

The primary challenge of the insulation technique was solved by using a novel MEMS fabrication technique to increase the thickness of the silicon dioxide. A high aspect-ratio lattice (column) structure was etched into the silicon thruster substrate using a deep reactive ion etcher (DRIE). This structure was then thermally oxidized to produce an insulating spacer an order of magnitude thicker than that which can be achieved with the thermal oxidation of silicon alone. A close-up picture of the insulation pattern is shown in Figure 3.

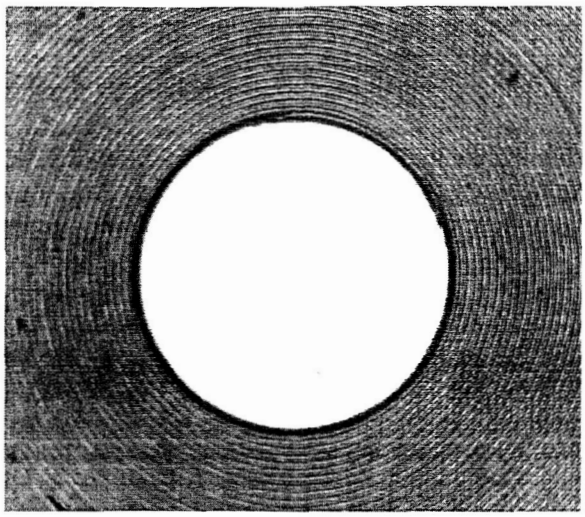

Figure 3. Closeup of the insulation.

Micro-thruster fabrication begins with a standard 10 cm diameter, 300-μm-thick double-side polished silicon wafer. The wafer is deposited with approximately 2000 Å of low-pressure chemical vapor deposited (LPCVD) silicon nitride. The nitride is then patterned with reactive ion etching (RIE) to create a mask to prevent oxidation in the area of the thruster nozzle. The wafer is then re-patterned with a thick photoresist mask (AZ 4620 or similar) to create a circular comb structure with 5 to 10 μm sidewalls (see Figure 3). This structure is transferred to the silicon with an 80 μm deep reactive ion etch (DRIE) using the Bosch process. Following photoresist removal, a long wet oxidation at 1000°C (approximately 72 hrs) is used to oxidize the silicon comb structure all the way through, thus providing electrical isolation from the high voltage electrode to the substrate. During fabrication, the thermal oxidation was measured on a flat test wafer to a depth of > 5 μm, which was sufficient to penetrate the wafer column from both sides.

Following this oxidation step, a 30 second buffered oxide dip removes oxide on the nitride in the nozzle area, and the nitride is removed with hot phosphoric acid (80°C.) The nozzle area is then recessed with a blanket DRIE step, with the rest of the wafer protected from etching by the previously grown thermal silicon dioxide. Next the wafer is mounted with wax on a Pyrex carrier wafer, and the wafer backside is patterned with AZ4620 with alignment to the front-side nozzle pattern (approximate tolerance 2 μm). Fluidic through holes (diameter 15-100 μm) are deep etched with a through-wafer etch using DRIE. The wafer is then removed from the Pyrex carrier wafer with an acetone soak, and the silicon dioxide protrusions are mechanically removed with a probe tip (indicated by the slash marks in step 6). Lastly, the devices are diced for testing. This process flow is illustrated here in Figure 4.

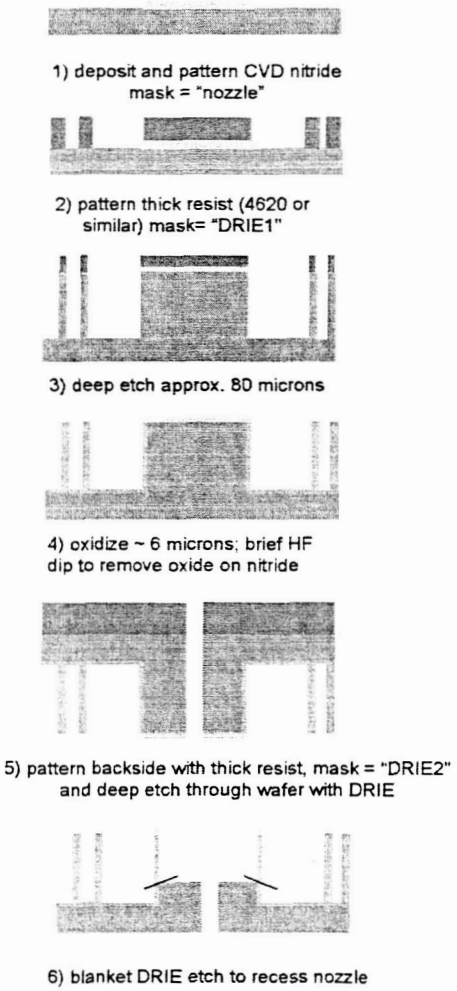

Figure 4. Process flow of the colloidal MEMS thruster fabrication.

A 50μm thick nickel annulus is placed on top of the insulation to serve as the extractor electrode. This electrode is connected to a negative constant-voltage power supply at approximately 3 kV. The backside of the emitter electrode is connected to a positive constant voltage supply at approximately 500 V. A cutaway schematic of the thruster emitter is shown in Figure 5.

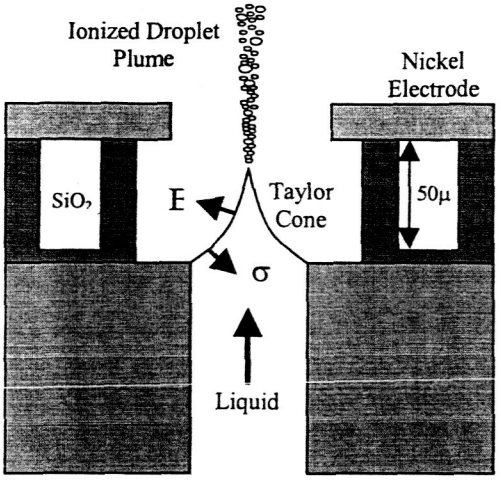

Figure 5. Cutaway schematic of the emitter.

Other researchers have attempted a similar "2-dimensional" fabrication method, including Martinez-Sanchez *et al.*, Stark *et al.*, and Paine *et al.* The 2-D array fabricated by Martinez-Sanchez *et al.* uses a non-traditional "wick" fabricated out of "black silicon" instead of a capillary to allow the fluid to flow up the outside of the emitter[14]. This configuration was reported to have significantly lower starting voltages[14]. The problem of increased evaporation from the exposed surfaces was mitigated by the use of EMI-BF_4 as a fuel[14], but external wetting of the surface does not lend itself to practical application for a spacecraft thruster. In addition to the 2-D array, Martinez-Sanchez *et al.* have fabricated a 1-dimensional array of slits with an integral propellant supply, and demonstrated operation of the array[14].

Stark *et al.* have also fabricated two-dimensional arrays and successfully produced large arrays of up to 20,000 capillary-shaped nozzles[15]. They have demonstrated electrical operations of their emitter design with emitters that are 100 μm ID and 400 μm OD with electrodes attached to the emitter, but they were not able to demonstrate operation of the devices as a thruster[16].

The work by Paine *et al.* used electrodes that were maintained in contact with the emitters. The researchers were able to produce insulators capable of holding 3 kV through 2 μm of thermal SiO_2, and 2 μm of CVD SiO_2, but were also not able to demonstrate operation of the devices[16].

Breakdown

Electrical breakdown for all MEMS devices is a persistent problem when high voltages are required, such as with a colloidal thruster. Thermal oxides can only be practically grown to thicknesses on the order of a few μm without requiring substantial processing times. Sputter deposition or chemical vapor deposited oxides can be grown to substantial thicknesses, up to approximately 5μm for CVD processes. Mueller *et al.* has studied CVD deposition in great detail for the purposes of grid fabrication[6].

The MEMS colloidal thrusters designed and demonstrated to date avoid the problem of electrical breakdown by physically separating the electrode from the emitter by using insulating packaging around the outside of the thruster[14,15]. The threshold of the electrical breakdown of the insulation in the NASA GSFC thruster was investigated as a function of pressure in a vacuum tank to examine the Paschen characteristics (Figure 6). The threshold below which breakdown cannot be initiated was tested to provide absolute stability limits for the colloidal thruster. An annular nickel electrode was placed on top of the insulation and electrical connections were made to the backside of the wafer and the electrode. The voltage on the electrode was increased steadily until a first discharge as noted by a small current draw by the electrode. The entire test assembly was contained in a vacuum tank, and the pressure was varied from atmospheric to 10^{-7} Torr.

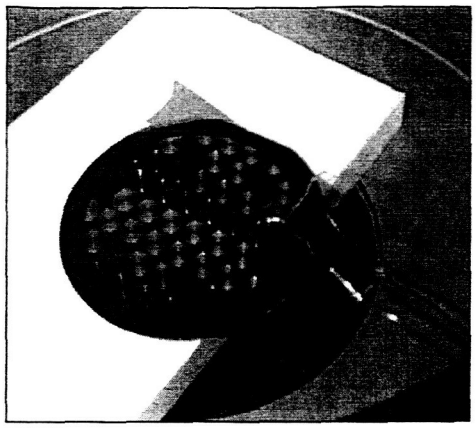

Figure 6. Breakdown test setup in vacuum.

In some cases, breakdown was allowed to continue to force a failure in the insulation to examine the damage. A picture of the damage caused by this "final" breakdown is shown in Figure 7. This final breakdown is suspected of being a bulk breakdown as described by Klein[17]. In this case, as can be seen from the figure, a gaseous discharge has overheated the SiO_2 column and caused the column to buckle.

Figure 7. Image of the effects of final breakdown on the insulation lattice.

An explanation of the breakdown behavior exhibited in Figure 6 is complex. One single mechanism could not explain all of the key features of the data, notably:

- From atmospheric pressure down to the "glow discharge" region (approximately 1 to 10^{-1} Torr), the breakdown voltage follows the Paschen breakdown curve of air. Insulators that have been damaged by final breakdown also follow the same trend with negligible decrease in performance.

- Below the glow discharge pressure, the breakdown voltage increases abruptly by an order of magnitude, far more than would be expected from a breakdown governed by the residual air.

- Within this regime of low pressure, insulators damaged by final breakdown show reduced breakdown thresholds.

The current hypothesis to explain this behavior is based on two different mechanisms. No single mechanism was found to explain the breakdown behavior at both atmospheric and vacuum pressures.

At atmospheric pressure, the breakdown mechanism is postulated to be across the "air" column (effectively a "surface flashover" through the gas within the gaps between the SiO_2 columns), and through the 5 μm of thermal oxide at the base of columns. The work by Mueller *et al.* shows a surface flashover breakdown strength of 20 V/μm. Considering the scatter on the data by Mueller *et al.*, the minimum onset breakdown strength should be ~10 V/μm for a gap distance of 50 μm[6]. This would yield a surface flashover voltage of approximately 500V for the 50 μm column height. The breakdown of the 5 μm thick thermal SiO_2 is also approximately 500 V, for a total breakdown along the discharge path of 1000 V. This corresponds to the result found experimentally in Figure 8.

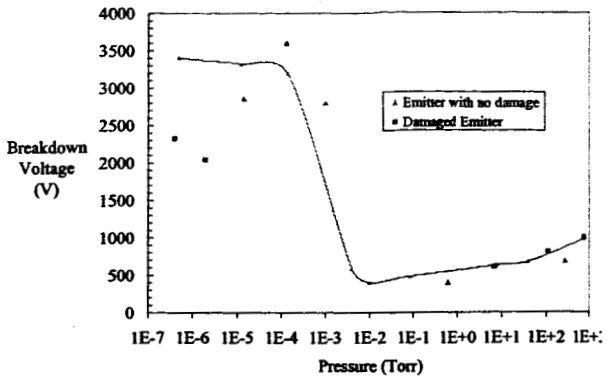

Figure 8. Minimum breakdown voltage of an emitter with 4μm thick columns.

As the pressure decreases, the minimum breakdown voltage also decreases, a trend opposite to that seen by Paine *et al.* and Mueller *et al*[6,7]. In their case, this suggested a surface breakdown mechanism, which suggests that the mechanism here is in fact dominated by discharge through the air column. At glow discharge pressures, the breakdown voltage of the air is essentially reduced to zero, and the breakdown is limited by the 500 V breakdown of the silicon dioxide at the base of the columns. For the cases where final breakdown has occurred, this is also accounted for by this mechanism since the air column is not affected by the final breakdown.

Below the glow pressure, a different mechanism is posited. The breakdown pressure peaks rapidly and reaches a plateau, instead of the constant gradual increase seen for the breakdown of air in the Paschen curve[18]. This is consistent with the results by Mueller *et al.* for a surface effect mechanism. Paine *et al.* also correctly note that a "surface flashover" would show Paschen characteristics (a change in breakdown voltage with pressure) – in this case it is a true surface effect, not a breakdown of residual gasses above the surface of the silicon dioxide column. The exact location of the breakdown in this case is not known, whether it is through the column, or along the surface of the column.

The effective minimum breakdown strength is approximately 60 V/μm based on the achieved breakdown values. Although this is comparable to the surface breakdown field strengths found by Mueller et al., the geometries used were considerably different. The breakdown voltages in this regime may also have been affected by surface contamination. Particles were confirmed by inspection to not be present, but some surface film contamination may have occurred, as no extreme measures were used to maintain cleanliness.

After breakdown, the insulation lattice is structurally damaged. Because of the buckling of the insulation column and deposition of electrode material, the breakdown was lowered to a value around 2 kV. This lowering of the breakdown voltage is consistent with a surface breakdown mechanism, since some material deposition takes place during the bulk mode discharge[6,17].

Experiment Setup

All of the testing has been performed in the glass bell jar shown in Figure 9. All of the hardware is insulated from the stand and mounted on a 1.25 cm thick Teflon plate. A vacuum flange is used as a propellant supply tank with pressurant gas (air) at atmospheric pressure. The propellant is delivered via a hypodermic tube and a Lee micro-valve. Propellant conductivities from 0.5 to 2 S/m have been measured for solutions with sodium iodide in formamide using a Myron L conductivity meter.

The static voltage is applied from both a Bertran power supply (negative) and an EMCO power supply (positive). The high voltages are routed through an ISI vacuum flange rated to 6000 VDC.

Images are captured by a Mitutoyo microscope in vacuum and captured by a high-resolution black and white 2/3" CCD camera. The microscope looses focus as pressure changes in the bell jar, but focus is readjusted by small displacements from a vacuum-rated Velmex positioning stage.

The prototype single emitters will be tested for performance using this setup. A Time Of Flight (TOF) diagnostic will also be used to measure the

amount of time required for droplets to reach a collector plate downstream of the emitter. This time can be used to determine the velocity of the droplets. Optical details of the Taylor cone will also be observed to compare to the computer model. Once a single emitter has been characterized, a complete array of emitters will be tested to verify the performance parameters.

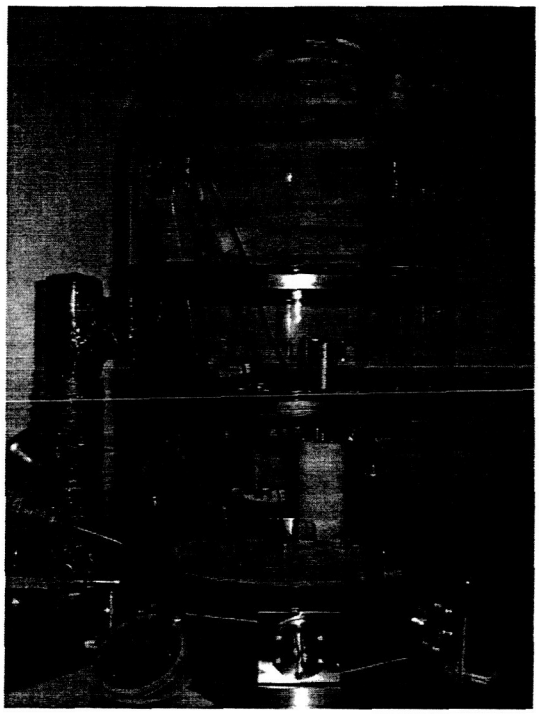

Figure 10. Picture of the test setup in the bell jar, with an undiced wafer in the foreground.

Computer Model

In addition to the design effort, a modeling effort was begun to examine the formation of the Taylor cone. G. I. Taylor showed that the equilibrium between surface tension and electric pressure results in a constant cone angle of 42.29 degrees[11]. However, it can be readily observed from his own experimental results that this assumption is an oversimplification, and it has been argued that the Taylor cone angle also changes with flow rate and the electrostatic field[19,20]. A constant cone angle would also results in infinite electric pressure and surface tension at the tip. In reality, this does not occur – at some finite radius, a discontinuity occurs, and the cone breaks down into a liquid jet.

De la Mora extended this theory by assuming the tip of the Taylor cone is an equipotential surface[20]. This equipotential surface can be described as the hyperboloid surface shown in Equation 3, where η is constant.

$$\eta = \left(\frac{\rho \sigma Q}{\gamma \varepsilon \varepsilon_0} \right) \tag{3}$$

In addition, the formation of the liquid jet has been shown experimentally to only occur above a certain critical instability criteria, η_{min}, shown here in Equation 4.

$$\eta_{min} = \sqrt{\frac{\rho}{\varepsilon_0}} \left(\frac{\Lambda_0 f}{1000 F \varepsilon} \right) \tag{4}$$

By combining the expressions for η and η_{min}, an expression for the flow rate Q at the tip of the cone can be obtained. The radius of curvature of the Taylor cone at the tip is a function of the radius of the jet. Since the radius of the liquid jet is a function of the mass flow rate, the expression in Equation 5 can be obtained for the equilibrium of the electric potential and the surface tension at the tip of the cone. Using the currently known values for formamide, this results in an electric field required for steady emission at the tip of E = 6.35 x 10^8 V/m. Further details of this derivation are described in Norgaard *et al*[21].

$$\frac{E_{Req}^2 \varepsilon_0}{2} = -\frac{\gamma}{R_C} \tag{5}$$

Most analytical work on the electric field published in the literature assumes a flat plate electrode. In reality, an annular electrode is needed to allow the liquid jet to pass through. To consider this, an axisymmetric model was created in FEMLAB to compute the electric field present at the tip of the Taylor cone[21]. Dirichelet boundary conditions ($V=V_0$) were applied at the

electrode surfaces, and the normal component of the electric field was set equal to zero at the boundary of axial symmetry. A mesh of 9063 nodes and 17888 triangular elements was created, with concentrated mesh densities around the cone and the electrode surfaces. The model was solved using a direct solver (UMPACK), and the electric field values were computed. Results in Norgaard et al. show the electrostatic fields for several different electrode and insulator configurations. For the design selected for testing, the voltage on the electrode required to reach the minimum electric field at the tip is 2050 VDC[21]. This voltage is readily achievable based on the breakdown voltage results shown here.

Conclusion

The NASA GSFC MEMS colloidal thruster has solved the problem of electrical breakdown to permit the integration of the electrode on top of the emitter by a novel MEMS fabrication technique. Devices have been successfully fabricated and the insulation properties have been tested to show they can support the required electric field of ~3000 VDC. A multi-physics model was created and used to verify that this voltage is sufficient to successfully operate the thruster. An experimental setup has been prepared to test the devices with both optical and Time-Of-Flight diagnostics.

Acronym List

CVD	Chemical Vapor Deposition
DRIE	Deep Reactive Ion Etch
EP	Electric Propulsion
GP-B	Gravity Probe - B
GSFC	Goddard Space Flight Center
LISA	Laser Interferometer Space Antenna
LPCVD	Low-Pressure Chemical Vapor Deposition
MAXIM	Micro-Arcsecond X-ray Interferometer Mission
MEMS	Micro-Electro-Mechanical System
NASA	National Aeronautics and Space Administration
PPU	Power Processing Unit
SIM	Space Interferometer Mission
TOF	Time-Of-Flight
TPF	Terrestrial Planet Finder

References

1. Laser Interferometer Space Antenna: A Cornerstone Mission for the Observation of Gravitational Waves, System and Technology Study Report, ESA-SCI(2000)11, July 2000.

2. Unwin, S., and R. Danner, The Space Interferometry Mission: Taking the Measure of the Universe, March 1999.

3. Cash, W., "MAXIM Preliminary Design", NASA Institute of Advanced Concepts, August 2000.

4. "Terrestrial Planet Finder(TPF): A NASA Origins Program to Search for Habitable Planets", NASA, JPL Publication 99-003, May 1999.

5. "The Technology Heritage of the Relativity Mission, Gravity Probe B", Buchman, S., Proceedings of the Eighth Marcel Grossman Meeting on General Relativity, 1999, pp. 1139-1150.

6. Mueller, J., D. Pyle, I. Chakraborty, R. Ruiz, W. Tang, C. Marrese, and R. Lawton, "Electric Breakdown Characteristics of Silicon Dioxide Films for use in Microfabricated Ion Engine Accelerator Grids", Micropropulsion For Small Spacecraft, Edited by M. Micci and A. Ketsdever, Progress in Astronautics and Aeronautics, Vol. 187, 2000, pp. 303-334.

7. Stark, J., B. Kent, R. Stevens, and M. Sandford, "Colloid Propulsion – A Re-evaluation, with an integrated design",

AIAA Paper # 2003-4851, 39th AIAA/ASME/ASME/SAE Joint Propulsion Conference, 20-23 July, 2003, Huntsville, AL.

8. Velasquez, L, J. Carretero, A. Ankinwande, and M. Martinez-Sanchez, "The concept and development of a micro-fabricated colloid thruster array", AIAA paper # 2003-4850, 39th AIAA/ASME/ASME/SAE Joint Propulsion Conference, 20-23 July, 2003, Huntsville, AL.

9. Zeleny, J., "The Electrical Discharge from Liquid Points, and A hydrostatic method of measuring the electric intensity at their surface", The Physical Review, Vol. III, No. 2, February 1914, pp. 69-91.

10. Norgren, C. T., and D. S. Goldin, "Experimental Analysis of the Exhaust Beam from a Colloid Thruster", NASA TM X-52035, 1964.

11. Taylor, G. I., and A. D. McEwan, "The stability of a horizontal fluid interface in a vertical electric field", *J. Fluid Mechanics*, 1965, Vol. 22, Part 1, pp. 1-15.

12. Hruby V., M. Gamero-Castaño, P. Falkos, and S. Shenoy, "Micro Newton Colloid Thruster System Development", 27th International Electric Propulsion Conference, Pasadena, CA, 15-19 October, 2001, IEPC Paper No. 01-281.

13. Gamero-Castaño, M., V. Hruby, D. Spence, N. Demmons, McCormick, R., C. Gasdaska, and P. Falkos, "Micro Newton Colloid Thruster for ST7-DRS Mission", 39th AIAA/ASME/SAE/ASEE Joint Propulstion Conference, Huntsville, AL, 2-23 July 2003, AIAA Paper No. 2003-4543.

14. Velasquez, L. F., J. A. Carretero, A. I. Ankinwande, and M. Martinez-Sanchez, "The Concept and Development of a Micro-fabricated Colloid Thruster Array", 39th AIAA/ASME/SAE/ASEE Joint Propulstion Conference, Huntsville, AL, 2-23 July 2003, AIAA Paper No. 2003-4850.

15. Stark, J., B. Stevens, and M. Alexander, "Fabrication and Operation of Micro-Fabricated Colloid Thruster Arrays", 39th AIAA/ASME/SAE/ASEE Joint Propulstion Conference, Huntsville, AL, 2-23 July 2003, AIAA Paper No. 2003-4852.

16. Paine, M. D., S. Gabriel, C. G. Schabmueller, and A. G. R. Evans, "Realisation of Very High Voltage Electrode-Nozzle Systems for MEMS", in publication, Sensors and Actuators.

17. Klein, N., *IEEE Trans. Electron. Devices*, ED-13, No. 11, 788, 1966.

18. Paschen, F, Wied. Ann., Vol. 37, 1889, pp. 69-96.

19. Covey, T. R., and D. Pinto, "Nanospray Electrospray Ionization Development", Applied Electrospray Mass Spectrometry, pp. 105-148, Edited by: B. Pramanik, A. Ganguly, and M. Gross, Marcel Dekker Inc., NY, 2002.

20. De la Mora, J. F., and I. G. Loscertales, "The current emitted by highly conducting Taylor cones", *J. Fluid Mechanics*, 1994, Vol. 260, pp. 155-184.

21. Norgaard, P. C., and E. H. Cardiff, "Finite Element Modeling of a MEMS Colloidal Thruster", AIAA Region VI Student Conference, 1-3 April, 2004, UCLA, CA.